energies

MDPI

Article

Multi-Cell-to-Multi-Cell Battery Equalization in Series Battery Packs Based on Variable Duty Cycle

Shengyi Luo, Dongchen Qin, Hongxia Wu *, Tingting Wang and Jiangyi Chen

School of Mechanical and Power Engineering, Zhengzhou University, Zhengzhou 450001, China; shengyi_luo1@163.com (S.L.); dcqin@zzu.edu.cn (D.Q.); wangtingting@zzu.edu.cn (T.W.); cjy1974@zzu.edu.cn (J.C.)

* Correspondence: wu_hx@zzu.edu.cn; Tel.: +86-187-3606-0839

Abstract: Batteries are widely used in our lives, but the inevitable inconsistencies in series-connected battery packs will seriously impact their energy utilization, cycle life and even jeopardize their safety in use. This paper proposes a balancing topology structure combining Buck-Boost circuit and switch array to reduce this inconsistency. This structure can realize multi-cell-to-multi-cell (MC2MC) battery balancing by controlling the switch array and having a fast balancing speed, easy expansion and few magnetic components. Then, the operation principle of the proposed balancing topology is analyzed, and the simulation model is verified. In addition, the effects of switching frequency and voltage difference on the equalization effect are further analyzed. The results show that the higher the switching frequency, the lower the time efficiency, but the higher the energy efficiency. The voltage difference significantly impacts the duty cycle, so it is absolutely necessary to introduce a variable duty cycle in the multi-cell-to-multi-cell equalization. Finally, eight series batteries are selected for simulation verification. The simulation results show that, compared with any-cell-to-any-cell (AC2AC) equalization, the time efficiency of multi-cell-to-multi-cell equalization is improved considerably, the energy efficiency is improved slightly, and the variance of the completed equalization is reduced, demonstrating the excellent performance of multi-cell-to-multi-cell equalization.

Keywords: lithium-ion battery; active equalization; multi-cell-to-multi-cell (MC2MC); variable duty cycle

Citation: Luo, S.; Qin, D.; Wu, H.; Wang, T.; Chen, J. Multi-Cell-to-Multi-Cell Battery Equalization in Series Battery Packs Based on Variable Duty Cycle. *Energies* **2022**, *15*, 3263. https://doi.org/10.3390/en15093263

Academic Editor: Sheldon Williamson

Received: 31 March 2022
Accepted: 27 April 2022
Published: 29 April 2022

1. Introduction

Considering energy security, environmental protection and technological progress, industries such as the global power grid, manufacturing and transportation have gradually turned to low energy consumption, low pollution and low carbon [1–3]. Lithium-ion batteries are widely used in electric vehicles, mobile communications, aerospace and energy storage systems [4–6] due to their high energy density, low self-discharge rate, long cycle life, small size, and lightweight [7]. In order to meet the high voltage, high power and large capacity requirements of electric vehicles and energy storage systems, batteries are often used in groups in series or parallel [8]. However, due to the complexity of lithium-ion battery manufacturing technology and production process, the capacity, voltage, internal resistance and other performance parameters of lithium-ion batteries produced in the same batch will still be inconsistent [9]. This inconsistency will be further deepened during use and storage [10]. According to the "bucket theory", the maximum charging capacity of the battery pack is limited by the highest SOC battery, and the maximum discharging capacity is limited by the smallest SOC battery. This makes the actual usable capacity of the battery pack smaller than the theoretical maximum usable capacity [11]. This phenomenon persists throughout the life cycle of the battery pack.

In order to reduce the energy difference between the individual cells of the battery pack, the battery balancing technology came into being. With the refinement of battery

modeling theory and the improvement of SOC estimation methods, the accuracy of battery models is becoming higher and higher [12,13], which provides a solid basis for research in areas such as battery equalization. The battery balancing system mainly includes balancing topology and control strategy [14]. The balancing topology is related to the dissipation or transfer of the balancing energy. Improving the topology can effectively improve the speed and efficiency of battery balancing, reduce circuit losses and lower balancing costs. There are various forms of balancing topology. According to whether the energy is dissipated in the balancing process, it can be divided into passive balancing (also called dissipative balancing) and active balancing (also called non-dissipative balancing) [15]. According to the energy transfer path in the equalization process, it can be divided into adjacent cell-to-cell (AC2C), pack-to-cell (P2C), cell-to-pack (C2P), any-cell-to-any-cell (AC2AC) and multi-cell-to-multi-cell (MC2MC) equalization methods [16].

Passive equalization refers to the technology of using parallel resistance to consume the batteries with more energy or higher voltage in the battery pack until the energy of each battery tends to be consistent [17]. Although passive equalization is easy to design and implement, it has the disadvantages of serious resistance heating effect, long equalization time and low energy utilization rate [18].

Active balancing transfers balancing energy from batteries with higher energy to batteries with lower energy through energy storage elements, which can meet the requirements of high efficiency, fast speed, and large current. It is the mainstream equalization scheme at present [19]. Given the different energy storage elements in the equalization process, it can be divided into four types of equalization topologies, capacitance-based [20–22], inductance-based, transformer-based [23–27] and converter based [28–35].

Pascual et al. [20] first proposed a multi-switched capacitor structure, but its balancing energy could only be transmitted between adjacent batteries through capacitors. Lee et al. [21] improved the switched capacitor equalization scheme and used zero-current switched capacitors to improve the equalization efficiency. Daowd et al. [22] proposed a single switched capacitor structure with a single capacitor as the energy storage element, and equalization energy could be transferred between any two cells. However, the capacitor-based balancing topology can only ensure the same voltage between batteries but cannot ensure the same energy. The balancing effect is poor when the battery voltage difference is not obvious. Thus, it is only suitable for occasions that do not require high equalization speed and accuracy.

In order to ensure the reliability of the balancing circuit under high voltage and high current conditions, transformer-based isolated balancing topologies are gaining more and more attention. It uses the transformer as the energy transfer carrier and transfers energy through mutual inductance. Li et al. [23] proposed a coaxial multi-winding transformer topology, but it could only realize the one-way transfer of balancing energy. Kutkut et al. [24] proposed an improved scheme for multi-secondary transformers, which could reduce the number of transformer secondary sides by half. Liu et al. [25] combined the switch array with the forward transformer and reduced conduction losses through synchronous rectification. But the magnetic reset circuit designed to prevent transformer core saturation complicated the topology and reduced reliability. Shang et al. [26] introduced forward transformation and flyback transformation into a multi-winding transformer simultaneously. The magnetic energy in the transformer at the end of each cycle was eliminated by the flyback transformation, which effectively solved the mismatch problem of the multi-winding transformer. In order to optimize the equalizer structure, Shang et al. [27] reduced the number of transformer windings by half by introducing a coupled half-bridge converter based on Reference [26], but it complicated the control process. Transformer-based equalization topologies are bulky, expensive, and difficult to expand; it is only suitable for occasions with few series batteries.

Using DC/DC converter circuits, such as the Cuk circuit, Boost circuit and Buck-Boost circuit to achieve equalization is called converter-based battery equalization, which also uses capacitors, inductors or inductors or transformers as energy storage elements.

Daowd et al. [28] compared a variety of active and passive equalization schemes in MATLAB/Simulink. They pointed out that the DC/DC converter equalization had high speed and high-efficiency advantages. Das et al. [29] proposed a distributed bidirectional active equalization structure based on a Buck-Boost converter. This structure used inductors as energy storage elements, but equalization energy could only be transferred between adjacent batteries in sequence. In [30], the first and last batteries were also connected with a basic Buck-Boost topology unit so that the batteries in series could form a circular energy loop, which increased the flexibility of balancing energy transfer. Wu et al. [31] proposed a hierarchical equalization topology based on the Buck-Boost converter. The equalization process was divided into multiple equalization processes of different layers according to the equalization energy flow. The equalization processes between different layers did not affect each other and could occur simultaneously to effectively speed up the equalization speed. Wang et al. [32] proposed an equalization topology that could construct multiple Buck-Boost converters between adjacent cells or adjacent cell clusters. The equalization path of this structure was flexible, and different equalization processes could occur simultaneously, so output power could be significantly improved by forming cell groups. However, the deficiency of reference [30–32] is that the equalization energy can only be transmitted successively between adjacent batteries (clusters). Chen et al. [33] proposed a bidirectional active equalization method based on a single inductor, which allowed equalization energy to be directly transferred from any cell to any cell. To optimize the equalization process, the influence of various factors on the equalization current and efficiency is then analyzed. Wu et al. [34] adopted a balancing topology combining a Cuk equalizer and double-layer selector switches, which could also achieve energy transfer between any battery. Although this topology reduced the number of inductors and capacitors exponentially, it required many switches. In order to equalize multiple cells simultaneously in one equalization process, Shang et al. [35] proposed a direct multi-cell-to-multi-cell equalization topology based on the matrix LC converter or the half-bridge LC converter to realize the direct energy transfer from continuous high-energy unit group to continuous low-energy unit group. However, this topology had a complex structure and required many switches. Converter-based equalization topology has low loss, high speed and good scalability, and it is one of the key development directions of active equalization.

In summary, the capacitor-based equalization topology is only suitable for occasions with low equalization speed and accuracy requirements. The inductance-based equalization topology is often combined with transformers and converters. The transformer-based equalization topology has a large volume, high cost and is not easy to expand. Therefore, this paper designs the balancing topology based on the Buck-Boost converter. The topology structure is simplified by introducing the switch array while realizing MC2MC equalization. According to the analysis results of the factors affecting the equalization effect, an equalization control strategy based on variable duty ratio is proposed. Finally, the simulation verification of eight series battery packs is carried out.

The structure of this paper is as follows. The second part introduces the topology and operating principle of MC2MC equalization based on the Buck-Boost circuit. The third part analyzes the factors that affect the equalization effect. The fourth part uses Matlab/Simulink to model and simulate the proposed topology and control strategy based on a variable duty cycle. Finally, the fifth section gives the relevant conclusions.

2. Equalization Circuit Analysis

2.1. Balancing Topology

This paper uses the Buck-Boost circuit combined with the switching array to design the equalization topology, which enables the equalization of the multi-cell-to-multi-cell energy transfer by controlling the switching array. The overall balancing topology is shown in Figure 1. The main structure of this topology is the switching array and the balancing main circuit. The switch array consists of positive switch S11, S21, S31~Sn1 and negative switch S12, S22, S32~Sn2. All positive switches are connected together to form a positive bus, and

all negative switches are connected to form a negative bus. The main balancing circuit adopts the non-isolated Buck-Boost circuit, and its circuit elements include inductance L and switching devices Q1, Q2, Q3 and Q4. The circuit operates under continuous current mode (CCM) to ensure that more energy is transferred in one switching cycle.

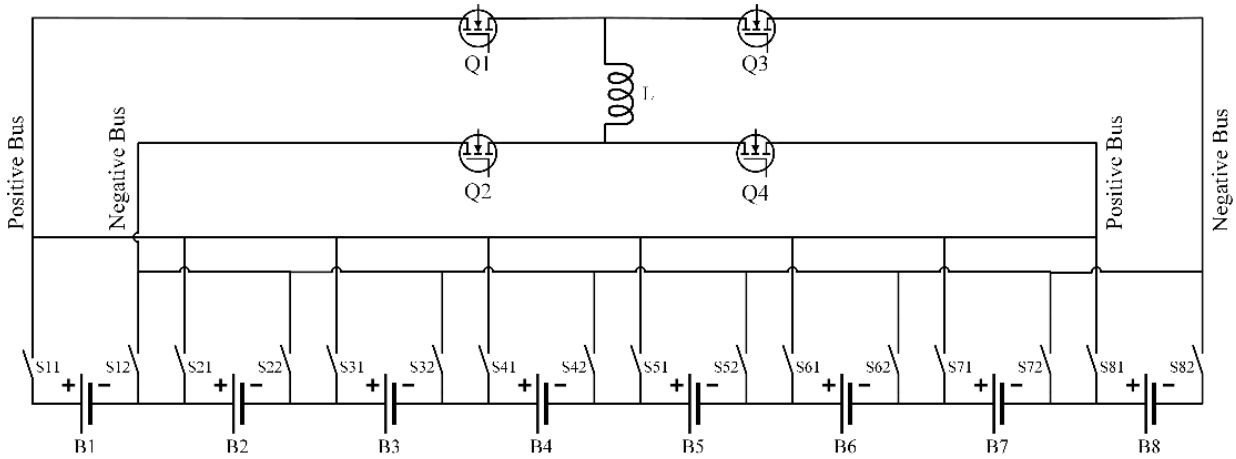

Figure 1. Main circuit of the proposed topology.

The proposed balancing topology has the following advantages.

(1) Multiple batteries can be equalized simultaneously in one equalization process, which greatly reduces the equalization time.
(2) Only additional positive and negative switches are needed when the number of series batteries increases. Thus, the circuit complexity remains unchanged; that is, the circuit is easy to expand.
(3) The number of magnetic components, such as inductance and capacitance, is greatly reduced.

2.2. Principle of Operation

The proposed topology has three typical working modes, namely any-cell-to-any-cell equalization (Mode 1), multi-cell-to-any-cell equalization (Mode 2) and multi-cell-to-multi-cell equalization (Mode 3). This paper takes eight series batteries as examples to analyze their working principle.

Mode 1: Assuming that the source battery B1 balances with the target battery B5, as shown in Figure 2, this process is divided into two steps.

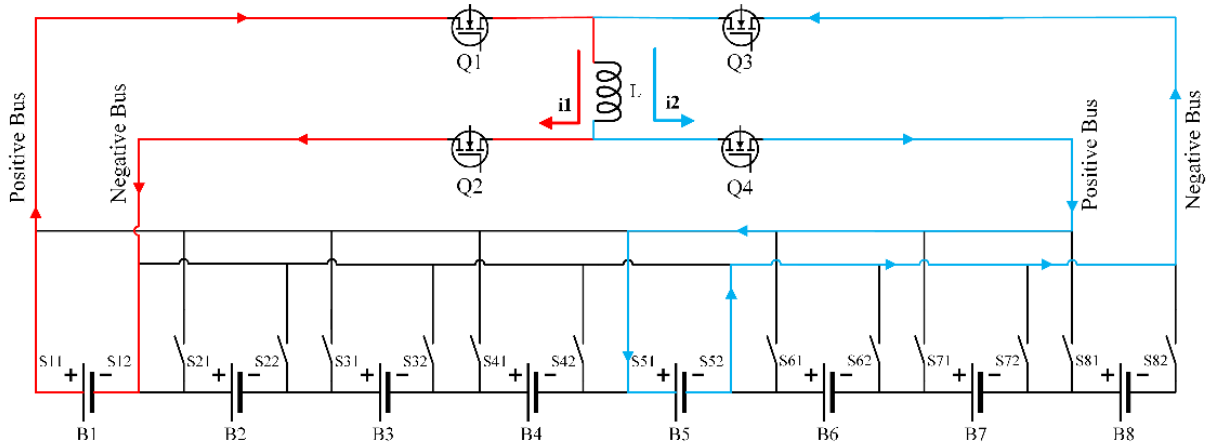

Figure 2. Any-cell-to-any-cell balancing.

1. Source battery B1 discharging: The discharging loop is composed of source battery B1, positive and negative switches S11, S12, MOS transistors Q1, Q2 and inductor L. The current flows along the red arrow. At this time, the electric energy of the source battery B1 is converted into the magnetic energy of the inductor L.
2. Target battery B5 charging: The charging loop consists of target battery B5, positive and negative switches S51, S52, MOS transistors Q3, Q4 and inductor L. The current flows along the blue arrow. At this time, the magnetic energy stored in the inductor L is converted into electric energy in the target battery B5.

Mode 2: Assuming that adjacent batteries B2 and B3 form a high-energy battery cluster to balance the target battery B5. As shown in Figure 3, this process is divided into the following two steps.

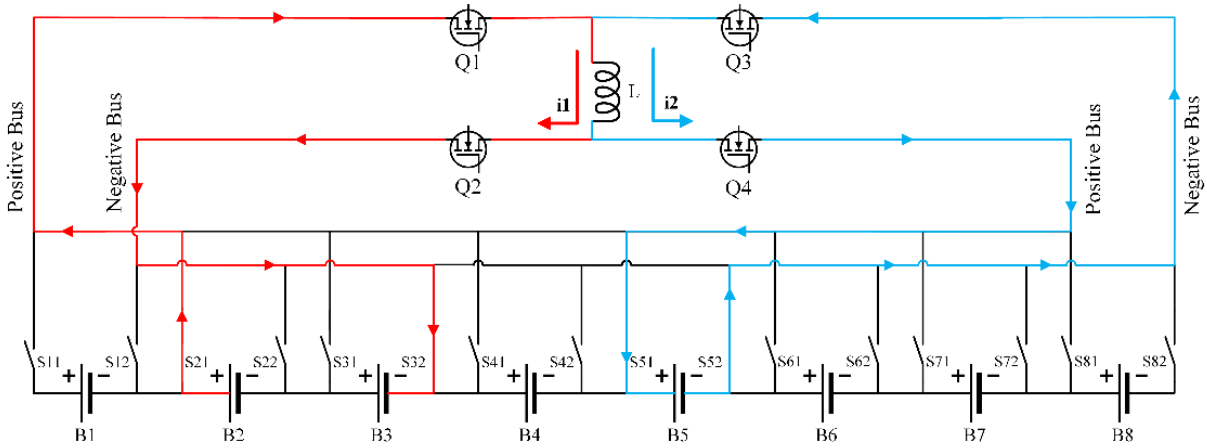

Figure 3. Multi-cell-to-any-cell balancing.

1. Battery clusters B2, B3 discharging: The discharging loop is composed of battery clusters B2 and B3, positive and negative switches S21 and S32, MOS transistors Q1, Q2 and inductor L. The current flows along the red arrow. At this time, the electrical energy of the high-energy battery cluster B2 and B3 is converted into the magnetic energy of the inductor L.
2. Target battery B5 charging: The charging loop consists of target battery B5, positive and negative switches S51, S52, MOS transistors Q3, Q4 and inductor L. The current flows along the blue arrow. At this time, the magnetic energy stored in the inductor L is converted into electric energy in the target battery B5.

Mode 3: Assuming that high-energy battery clusters B2 and B3 balance with low-energy battery clusters B6 and B7. As shown in Figure 4, this process is divided into the following two steps.

1. Battery clusters B2, B3 discharging: The discharging loop is composed of battery clusters B2 and B3, positive and negative switches S21, S32, MOS transistors Q1, Q2 and inductor L. The current flows along the red arrow. At this time, the electrical energy of the high-energy battery cluster B2 and B3 is converted into the magnetic energy of the inductor L.
2. Battery clusters B6, B7 charging: The charging loop consists of battery clusters B6 and B7, positive and negative switches S61, S72, MOS transistors Q3, Q4 and inductance L. The current flows along the blue arrow. At this time, the magnetic energy stored in the inductor L is converted into electrical energy in the low-energy battery cluster B6 and B7.

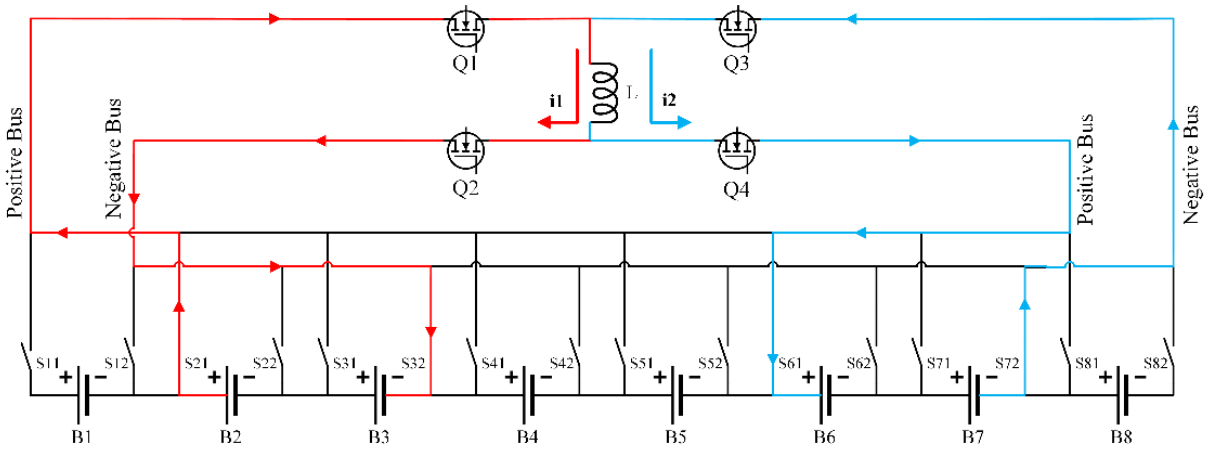

Figure 4. Multi-cell-to-multi-cell balancing.

2.3. Simulation Model Verification

The accuracy of the established Matlab/Simulink simulation model is verified by the equivalent circuit model of the proposed balancing topology. A simplified equivalent model of the main circuit is shown in Figure 5. Figure 6 shows its switch transistor gate drive signal. For ease of analysis, we assume that the switch is ideal.

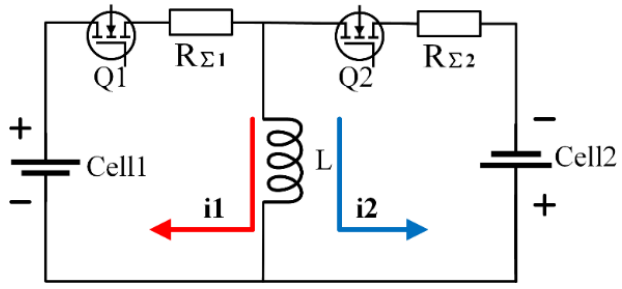

Figure 5. Equivalent model of the main circuit.

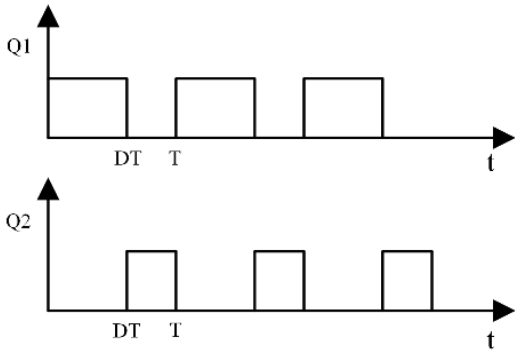

Figure 6. Drive signal waveform of MOS transistors.

Assuming that batteries Cell1 and Cell2 are the source and target batteries, respectively. The equalization process is divided into the following two steps.

Step 1 [0~DT]: At this time, the switch transistor Q1 is turned on, and Q2 is turned off. Source battery Cell1 charges inductor L. The red arrow shows the current path. The expression of the discharging current $i_1(t)$ of the source battery Cell1, that is, the charging current $i_L(t)$ of the inductor L is given by

$$i_1(t) = i_L(t) = \frac{E_1}{R_{\Sigma 1}}\left(1 - e^{-\frac{R_{\Sigma 1}}{L}t}\right) \quad 0 \le t \le DT \tag{1}$$

Step 2 [DT~T]: At this time, the switch transistor Q2 is turned on, and Q1 is turned off. Inductor L charges the target battery Cell2. The blue arrow shows the current path. The expression of the charging current $i_2(t)$ of the target battery Cell2, that is, the discharging current $i_L(t)$ of the inductor L is given by

$$i_2(t) = i_L(t) = \frac{E_1}{R_{\Sigma 1}}(1 - e^{-\frac{R_{\Sigma 1}}{L}DT})e^{-\frac{R_{\Sigma 2}}{L}(t-DT)} - \frac{E_2}{R_{\Sigma 2}}(1 - e^{-\frac{R_{\Sigma 2}}{L}(t-DT)}) \qquad DT \le t \le T \tag{2}$$

where, E_1 is the voltage of the source battery Cell1 (V), E_2 is the voltage of the target battery Cell2 (V), $R_{\Sigma 1}$ is the total resistance of the discharging loop (Ω), $R_{\Sigma 2}$ is the total resistance of the charging loop (Ω) (both including the on-resistance of the MOSFET, the equivalent resistance of the inductance, the equivalent resistance of the wire and the internal resistance of the battery), L is the inductance value of the inductor L (H), D is the duty cycle of the PWM control signal and T is the switching period of the switching transistor (s).

$T = \frac{1}{f}$, where, f is switching frequency (Hz).

Since the circuit works in continuous current mode, in order to avoid magnetic saturation of the inductor, the charging current $i_2(t)$, that is, the inductor's current $i_L(t)$ must be zero at the end of each cycle. This can be expressed by the following equation.

$$i_2(T) = i_L(T) = 0 \tag{3}$$

This can be simplified to (4).

$$\frac{E_1 R_{\Sigma 2}}{E_2 R_{\Sigma 1}} = \frac{1 - e^{-\frac{R_{\Sigma 2}}{L}(1-D)T}}{(1 - e^{-\frac{R_{\Sigma 1}}{L}DT})e^{-\frac{R_{\Sigma 2}}{L}(1-D)T}} \tag{4}$$

Assuming that the source battery voltage $E_1 = 3.45$ V, the target battery voltage $E_2 = 3.2$ V, the inductor $L = 100$uH, the switching frequency $f = 10$ KHz and the discharging and charging loop resistance $R_{\Sigma 1} = R_{\Sigma 2} = 0.2$ Ω. Substituting the above parameters into Equation (4) gives a duty cycle of $D = 0.506$.

The calculated value of inductor current can be obtained by substituting the above parameter data into Equations (1) and (2). The simulated value of inductor current can be obtained by substituting into the Simulink simulation model of the equivalent circuit. The results are represented in Figure 7.

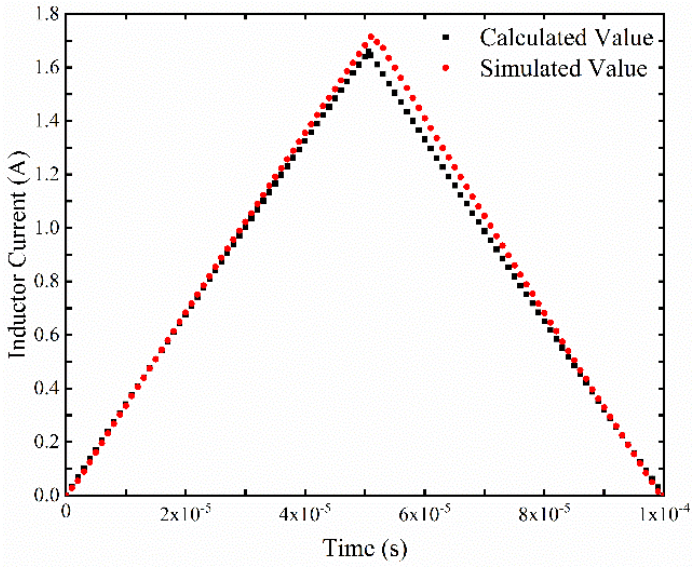

Figure 7. Calculated and simulated values of inductor current in a single cycle.

It can be seen from Figure 7 that the inductive current changes approximately linearly during battery equalization. The calculation results show that the maximum inductor current is generated at $t = 5.06 \times 10^{-5}$, which is 1.6603 A. The simulation shows a maximum current at $t = 5.1 \times 10^{-5}$, which is 1.7143 A. The relative error between them is 3.25%, but this is due to the simulation time step setting. In practice, the maximum inductive current should occur at $t = DT$ and be less than the simulated maximum value. After that, the inductor current decreases and decreases to zero at the end of the cycle. The results show the simulation model can truly express the equalization process.

3. Analysis of Factors Affecting the Equalization Effect

Equalization speed and efficiency are two basic indexes to judge the quality of an equalization system. When a certain amount of charge needs to be transferred to the target cell, the larger the average equalization current, the faster the equalization speed, the lower the heat loss caused by the loop resistance and the higher the equalization efficiency. From Equations (1) and (2), we can find that the average values of the source battery discharging current $i_1(t)$ and the target battery charging current $i_2(t)$ over the entire period T and in the respective discharging cycle DT and charging cycle $(1-D)T$ are given by

$$\overline{i_1} = \frac{\int_0^{DT} i_1(t)dt}{T} = \frac{E_1 D}{R_{\Sigma 1}} + \frac{LE_1}{R_{\Sigma 1}^2 T}(e^{-\frac{R_{\Sigma 1}}{L}DT} - 1) \tag{5}$$

$$\overline{i_2} = \frac{\int_{DT}^{T} i_2(t)dt}{T} = \frac{LE_1(1-e^{-\frac{R_{\Sigma 1}}{L}DT})(1-e^{-\frac{R_{\Sigma 2}}{L}(1-D)T})}{R_{\Sigma 1}R_{\Sigma 2}T} + \frac{LE_2(1-e^{-\frac{R_{\Sigma 2}}{L}(1-D)T})}{R_{\Sigma 2}^2 T} - \frac{E_2(1-D)}{R_{\Sigma 2}} \tag{6}$$

$$\overline{i_1}' = \frac{\int_0^{DT} i_1(t)dt}{DT} = \frac{E_1}{R_{\Sigma 1}} + \frac{LE_1}{R_{\Sigma 1}^2 DT}(e^{-\frac{R_{\Sigma 1}}{L}DT} - 1) \tag{7}$$

$$\overline{i_2}' = \frac{\int_{DT}^{T} i_2(t)dt}{(1-D)T} = \frac{LE_1(1-e^{-\frac{R_{\Sigma 1}}{L}DT})(1-e^{-\frac{R_{\Sigma 2}}{L}(1-D)T})}{R_{\Sigma 1}R_{\Sigma 2}(1-D)T} + \frac{LE_2(1-e^{-\frac{R_{\Sigma 2}}{L}(1-D)T})}{R_{\Sigma 2}^2(1-D)T} - \frac{E_2}{R_{\Sigma 2}} \tag{8}$$

where, $\overline{i_1}$ and $\overline{i_2}$ are the average values of the discharging current $i_1(t)$ and the charging current $i_2(t)$ over the entire period T, respectively. $\overline{i_1}'$ and $\overline{i_2}'$ are the average values of the discharging current $i_1(t)$ and the charging current $i_2(t)$ in respective discharging cycle DT and charging cycle $(1-D)T$, respectively. E_1 and E_2 are the voltages of the source battery Cell1 and the target battery Cell2. $R_{\Sigma 1}$ and $R_{\Sigma 2}$ are the total resistance of the discharging and charging circuits. L is the inductance value, D is the duty cycle and T is the switching period.

Heat loss rate due to equivalent resistances $R_{\Sigma 1}$ and $R_{\Sigma 2}$ is given by

$$W_1 = \int_0^{DT} E_1 i_1(t)dt = \frac{E_1^2}{R_{\Sigma 1}^2}[R_{\Sigma 1}DT + L(e^{-\frac{R_{\Sigma 1}}{L}DT} - 1)] \tag{9}$$

$$W_{R_{\Sigma 1}} = \int_0^{DT} {i_1}^2(t)R_{\Sigma 1}dt \tag{10}$$

$$W_{R_{\Sigma 2}} = \int_{DT}^{T} {i_2}^2(t)R_{\Sigma 2}dt \tag{11}$$

$$\eta_{re} = \frac{W_{R_{\Sigma 1}} + W_{R_{\Sigma 2}}}{W_1} \tag{12}$$

where, W_1 is the energy released by the source battery in one switching cycle. $W_{R_{\Sigma 1}}$ and $W_{R_{\Sigma 2}}$ are the heat dissipation energy caused by the equivalent resistors $R_{\Sigma 1}$ and $R_{\Sigma 2}$ in the discharging loop and the charging loop, respectively. η_{re} represents the percentage of heat loss energy caused by all equivalent resistors in the energy released by the source battery.

From Equations (5)–(12), we can know that the average equalization current and heat loss rate are affected by the source battery and target battery voltages E_1 and E_2, duty cycle D, switching frequency f and charging and discharging loop resistors $R_{\Sigma 1}$ and $R_{\Sigma 2}$. According to practical experience, the larger the equivalent resistance, the lower the time efficiency and energy efficiency. In addition, since the circuit operates in continuous current mode, the duty cycle D is determined by Equation (4). Therefore, the influence of the switching frequency f and the battery voltages E_1 and E_2 on the equalization effect is analyzed below.

3.1. Influence of Switching Frequency on Equalization Effect

3.1.1. Influence of Switching Frequency on Duty Cycle

Assuming that the source battery voltage $E_1 = 3.45$ V, the target battery voltage $E_2 = 3.2$ V, the inductor $L = 100$ uH and the discharging and charging loop resistance $R_{\Sigma 1} = R_{\Sigma 2} = 0.2\ \Omega$. The relationship between the duty ratio D and the switching frequency f can be obtained by Equation (4), as shown in Figure 8, and the values are shown in Table 1.

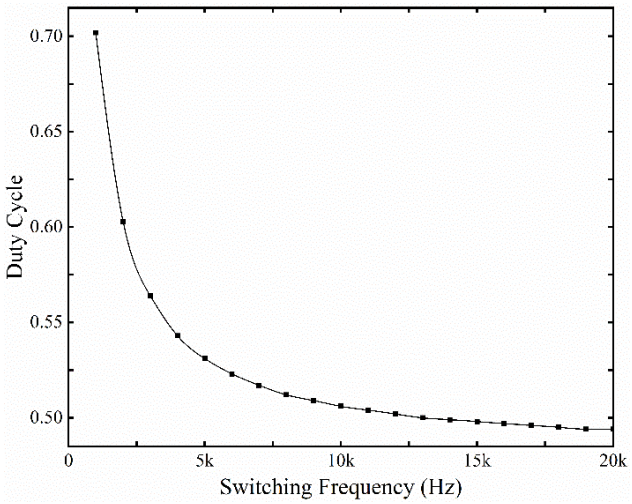

Figure 8. Relationship between duty cycle and switching frequency.

Table 1. Values of duty cycle at different switching frequencies.

Switching Frequency	1 k	2 k	3 k	4 k	5 k	6 k	7 k	8 k	9 k	10 k
Duty Cycle	0.702	0.603	0.564	0.543	0.531	0.523	0.517	0.512	0.509	0.506
Switching Frequency	11 k	12 k	13 k	14 k	15 k	16 k	17 k	18 k	19 k	20 k
Duty Cycle	0.504	0.502	0.5	0.499	0.498	0.497	0.496	0.495	0.494	0.494

It can be found from Figure 8 and Table 1 that the duty cycle decreases with the increase of switching frequency. In addition, as the switching frequency increases, the rate of change of the duty cycle gradually decreases to zero. That is, the duty cycle gradually tends to a certain limit value.

3.1.2. Influence of Switching Frequency on Average Equalizing Current

Assuming that the source battery voltage $E_1 = 3.45$ V, the target battery voltage $E_2 = 3.2$ V, the inductor $L = 100$ uH and the discharging and charging loop resistance $R_{\Sigma 1} = R_{\Sigma 2} = 0.2\ \Omega$. By substituting the switching frequency f and its corresponding duty cycle D obtained in Section 3.1.1 into Equations (5) and (6) can obtain the variation of the average equalization current with the switching frequency, as shown in Figure 9.

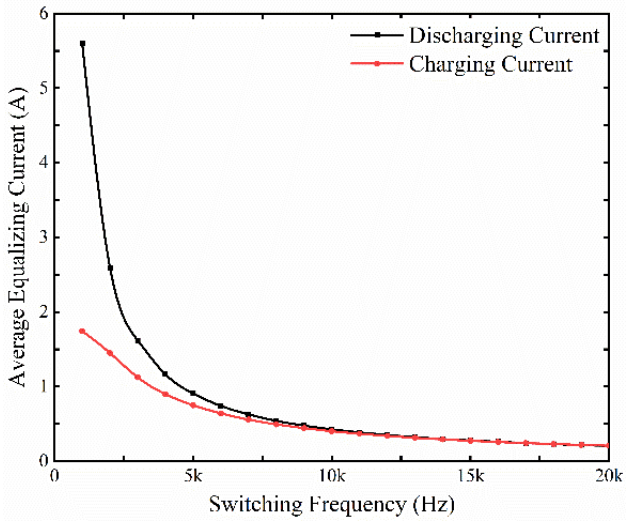

Figure 9. Variation of average equalizing current with switching frequency.

Figure 9 shows the average values $\overline{i_1}$ and $\overline{i_2}$ of the discharging current $i_1(t)$ and the charging current $i_2(t)$ in the whole period T decreased with the increase of the switching frequency f. For comparison at the same scale, the equation for the amount of charge q_2 transferred to the target battery Cell2 per unit time can be derived as Equation (13). The amount of charge transferred to the target cell Cell2 per unit time at different switching frequencies is obtained by substituting the corresponding parameter data, as shown in Figure 10.

$$q_2 = \int_{DT}^{T} i_2(t)dt \cdot f = \left(\frac{LE_1\left(1-e^{-\frac{R_{\Sigma 1}}{L}DT}\right)\left(1-e^{-\frac{R_{\Sigma 2}}{L}(1-D)T}\right)}{R_{\Sigma 1}R_{\Sigma 2}} + \frac{LE_2\left(1-e^{-\frac{R_{\Sigma 2}}{L}(1-D)T}\right)}{R_{\Sigma 2}^2} - \frac{E_2(1-D)T}{R_{\Sigma 2}}\right) \cdot f \quad (13)$$

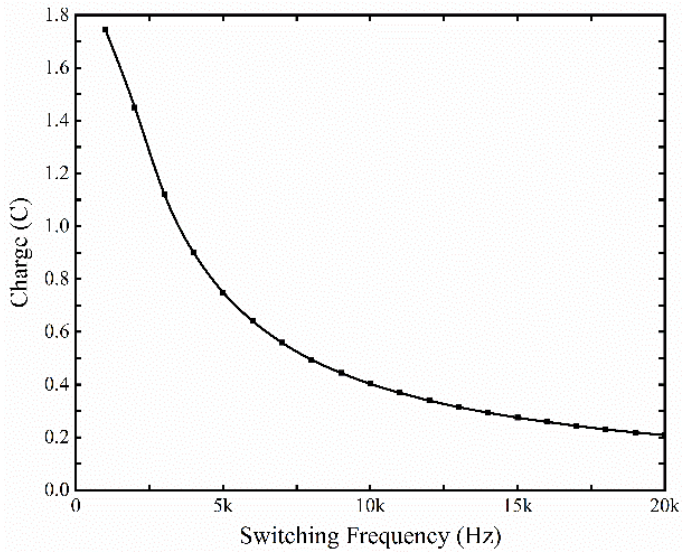

Figure 10. The amount of charge transferred to Cell2 at different switching frequencies.

Figure 10 shows as the switching frequency increases, the amount of charge per unit time transferred to the target cell Cell2 decreases and tends to a certain limit. Therefore, from the point of view of increasing the equalization current and improving the time efficiency, the switching frequency should be chosen as a smaller value.

3.1.3. Influence of Switching Frequency on Heat Loss Rate

Assuming that the source battery voltage $E_1 = 3.45$ V, the target battery voltage $E_2 = 3.2$ V, the inductor $L = 100$ uH and the discharging and charging loop resistance $R_{\Sigma 1} = R_{\Sigma 2} = 0.2\ \Omega$. By substituting the switching frequency f and its corresponding duty cycle D obtained in Section 3.1.1 into Equations (9)–(12) can obtain the variation of the heat loss rate with the switching frequency, as shown in Figure 11.

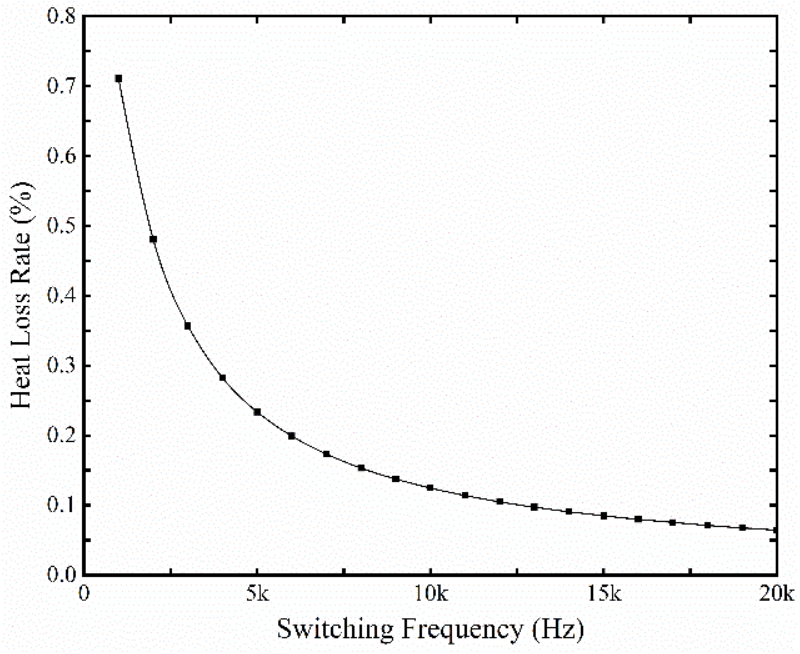

Figure 11. Variation of heat loss rate with switching frequency.

It can be seen from Figure 11 that the higher the switching frequency, the lower the heat loss rate, and it tends to a constant value. Therefore, selecting a medium frequency switch is beneficial to improving the equalization circuit's energy efficiency while reducing the hardware cost. Given that later studies show that equalization time can be significantly reduced by MC2MC equalization, the switching frequency $f = 10$ KHz is chosen in this paper to reduce hardware costs and improve the energy efficiency of the equalization circuit.

3.2. Influence of Voltage Difference on Equalization Effect

3.2.1. Influence of Voltage Difference on Duty Cycle

The voltage difference ΔE refers to the difference between the source battery voltage E_1 and the target battery voltage E_2 during the equalization process. It is given by

$$\Delta E = E_1 - E_2 \tag{14}$$

Compared with realizing the AC2AC equalization path, the MC2MC equalization method will produce a large voltage difference between the source and target batteries. This voltage difference will change in the equalization process. Assuming that the target battery voltage $E_2 = 3.2$ V, the inductor $L = 100$ uH, the switching frequency $f = 10$ KHz and the discharging and charging loop resistance $R_{\Sigma 1} = R_{\Sigma 2} = 0.2\ \Omega$. The relationship between the duty cycle D and the voltage difference ΔE can be obtained by Equation (4), as shown in Figure 12, and the partial values are shown in Table 2.

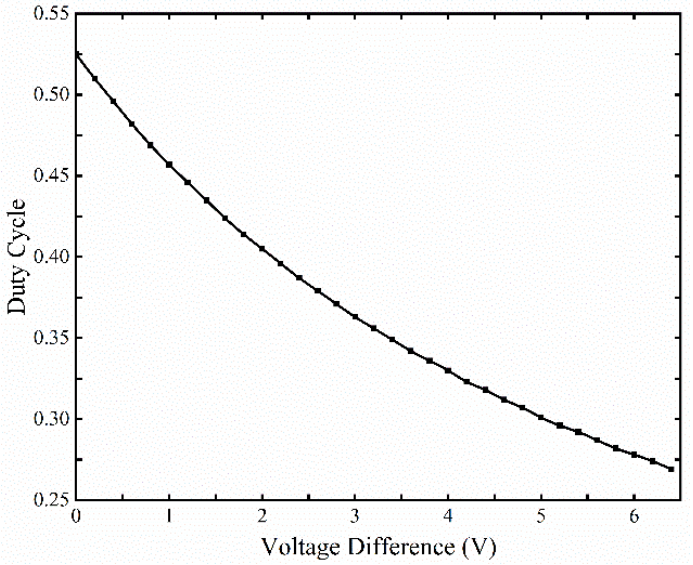

Figure 12. Variation of duty cycle with voltage difference.

Table 2. Partial values of duty cycle at different voltage differences.

Voltage Difference	0	0.8	1.6	2.4	3.2	4	4.8	5.6	6.4
Duty Cycle	0.525	0.469	0.424	0.387	0.356	0.33	0.307	0.287	0.269

It can be found from Figure 12 and Table 2 that the duty cycle decreases as the voltage difference increases. When one battery is balancing to one battery ($\Delta E = 0$), the duty cycle is 0.525. When two batteries are balancing to one battery ($\Delta E = 3.2$), the duty cycle is 0.356. When three batteries are balancing to one battery ($\Delta E = 6.4$), the duty cycle is 0.269. Therefore, in the MC2MC equalization system, the change in the duty cycle caused by the change in the voltage difference cannot be ignored; it is necessary to introduce a variable duty ratio.

3.2.2. Influence of Voltage Difference on Average Balancing Current

Assuming that the target battery voltage $E_2 = 3.2$ V, the inductor $L = 100$ uH, the switching frequency $f = 10$ KHz and the discharging and charging loop resistance $R_{\Sigma 1} = R_{\Sigma 2} = 0.2\ \Omega$. By substituting the voltage difference ΔE and its corresponding duty cycle D obtained in Section 3.2.1 into Equations (7) and (8) can obtain the variation of the average balancing current with the voltage difference, as shown in Figure 13.

Figure 13 shows the average values $\overline{i_1}'$ and $\overline{i_2}'$ of discharging current $i_1(t)$ and charging current $i_2(t)$ in their respective discharging and charging cycles increase with the increase of voltage difference. Based on the transfer of the same amount of charge to the target battery Cell2, the rate of improvement of the equalization time by increasing the voltage difference can be calculated. It is given by

$$\overline{i_2}'(1) \cdot (1 - D_1) \cdot T \cdot X_1 = \overline{i_2}'(2) \cdot (1 - D_2) \cdot T \cdot X_2 \tag{15}$$

where, $\overline{i_2}'(1)$, D_1 and X_1 respectively represent the average value, duty cycle and required number of cycles of the charging current $i_2(t)$ under a certain voltage difference. $\overline{i_2}'(2)$, D_2 and X_2 respectively represent the average value, duty cycle and required number of cycles of the charging current $i_2(t)$ under another voltage difference.

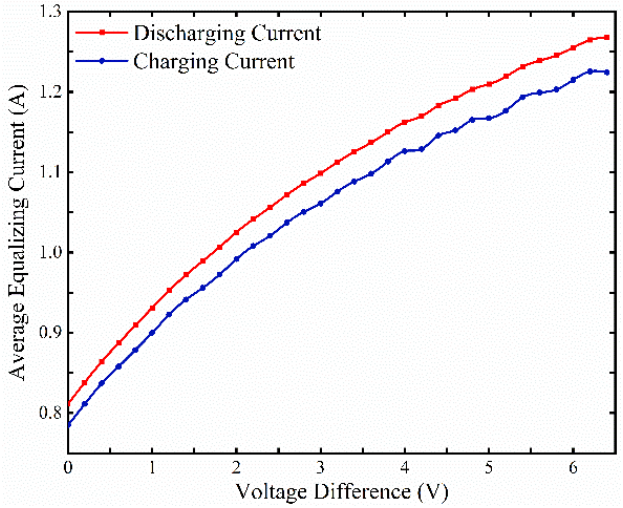

Figure 13. Variation of average equalizing current with voltage difference.

(1) The time improvement rate of the two-to-one battery equalization than the one-to-one battery equalization.

Substituting $\overline{i_2}'(1) = 0.7849$, $D_1 = 0.525$ as well as $\overline{i_2}'(2) = 1.0759$, $D_2 = 0.356$ into Equation (15) gives the following result.

$$X_2 = 0.538 \cdot X_1$$

It shows that under the condition of transferring the same amount of charge to the target battery, using two batteries to balance one battery, the time efficiency is improved by 46.2% compared to using only one battery to balance one battery.

(2) The time improvement rate of the three-to-one battery equalization than the two-to-one battery equalization.

Substituting $\overline{i_2}'(1) = 1.0759$, $D_1 = 0.356$ as well as $\overline{i_2}'(2) = 1.2244$, $D_2 = 0.269$ into Equation (15) gives the following result.

$$X_2 = 0.7742 \cdot X_1$$

It shows that under the condition of transferring the same amount of charge to the target battery, using three batteries to balance one battery, the time efficiency is improved by 22.58% compared to using two batteries to balance one battery.

(3) The time improvement rate of the three-to-one battery equalization than the one-to-one battery equalization.

Substituting $\overline{i_2}'(1) = 0.7849$, $D_1 = 0.525$ as well as $\overline{i_2}'(2) = 1.2244$, $D_2 = 0.269$ into Equation (15) gives the following result.

$$X_2 = 0.4165 \cdot X_1$$

It shows that under the condition of transferring the same amount of charge to the target battery, using three batteries to balance one battery, the time efficiency is improved by 58.35% compared to using only one battery to balance one battery.

To further illustrate the tendency of the voltage difference to enhance the equalization time, the amount of charge Q_2 received by the target cell in one cycle is derived for different voltage differences. It is given by Equation (16). By substituting the parameter data into the above equation, the relationship between the amount of charge Q_2 received by the target battery, and the voltage difference in a cycle can be obtained in Figure 14.

$$Q_2 = \int_{DT}^{T} i_2(t)dt = \frac{LE_1(1-e^{-\frac{R_{\Sigma 1}}{L}DT})(1-e^{-\frac{R_{\Sigma 2}}{L}(1-D)T})}{R_{\Sigma 1}R_{\Sigma 2}} + \frac{LE_2(1-e^{-\frac{R_{\Sigma 2}}{L}(1-D)T})}{R_{\Sigma 2}^2} - \frac{E_2(1-D)T}{R_{\Sigma 2}} \quad (16)$$

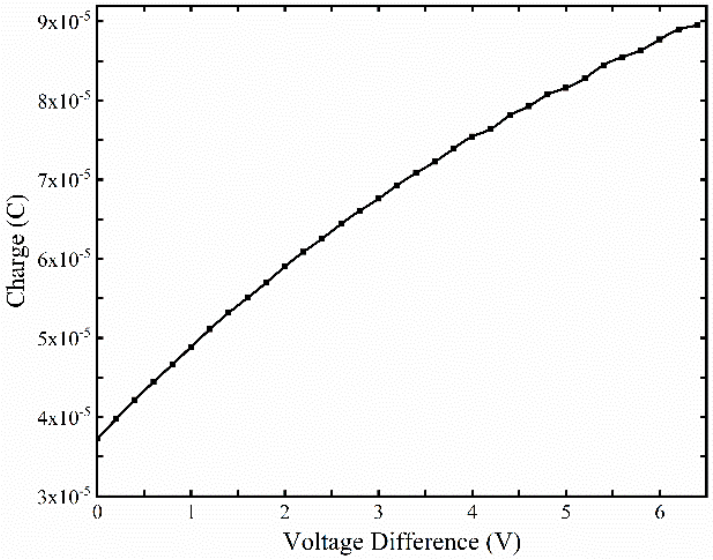

Figure 14. The amount of charge transferred to Cell2 at different voltage differences.

Figure 14 shows that as the voltage difference increases, the amount of charge received by the target battery in one period also increases accordingly. Therefore, the MC2MC equalization method can effectively reduce the equalization time and improve the time efficiency.

3.2.3. Influence of Voltage Difference on Heat Loss Rate

Assuming that the target battery voltage $E_2 = 3.2$ V, the inductor $L = 100$ uH, the switching frequency $f = 10$ KHz and the discharging and charging loop resistance $R_{\Sigma 1} = R_{\Sigma 2} = 0.2\ \Omega$. Substituting the voltage difference and its corresponding duty cycle obtained in Section 3.2.1 into Equations (9) to (12) can obtain the variation of the heat loss rate with the voltage difference, as shown in Figure 15.

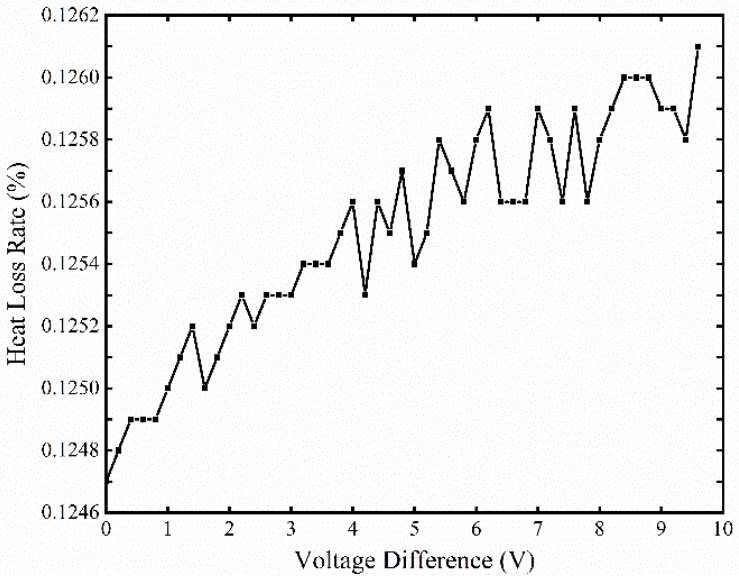

Figure 15. Variation of heat loss rate with voltage difference.

It can be seen from Figure 15 that the heat loss rate and the voltage difference are positively correlated. The heat loss rate η_{re1} of one-to-one battery equalization is 12.47%. The heat loss rate η_{re2} of two-to-one battery equalization is 12.54%. The heat loss rate η_{re3} of three-to-one battery equalization is 12.56%. The increase in heat loss rate is small, so the equalization method of MC2MC can effectively shorten the equalization time. The increase in heat loss is small, which has the dual advantages of high time efficiency and high energy efficiency.

4. Simulation Verification and Analysis

4.1. Balancing Control Strategy

In this paper, eight series batteries are selected for equalization simulation verification. The simulation model of this topology is established in MATLAB/Simulink2021a, including battery module, switching array, Buck-Boost equalization unit, switching control module and duty cycle control module based on voltage difference. The duty cycle control module determines the duty cycle in the MC2MC equalization process. SOC is selected as the equalization variable. Firstly, the initial charge state of each cell is used to determine whether a multi-cell cluster can be formed in the series battery pack. If the battery cluster cannot be formed, the AC2AC balancing strategy is performed, as shown in Figure 16a; otherwise, the MC2MC balancing strategy is performed, as shown in Figure 16b. In order to prevent the starting condition of the equalization circuit from being quickly satisfied again after the equalization of the battery pack is completed, the equalization start threshold Th_1 and the equalization termination threshold Th_2 are respectively set. In this paper, the start threshold Th_1 is 3, and the termination threshold Th_2 is 1.

4.2. Multi-Cell-to-Any-Cell Simulation Verification

Assuming that the SOC values of the eight series batteries are 42.3, 43.8, 42, 46.5, 44.5, 45.8, 46.2, and 42.5, respectively, and the energy state distribution diagram of the battery pack is shown in Figure 17. If the SOC value of a battery meets $SOC_j \geq \frac{\sum_{i=1}^{8} SOC_i}{8} + \frac{Th_2}{2}$, this battery is a high-energy battery, which is represented by yellow. If the SOC value of a battery meets $SOC_j \leq \frac{\sum_{i=1}^{8} SOC_i}{8} - \frac{Th_2}{2}$, this battery is a low-energy battery, which is represented by red. The remaining batteries are normal batteries, indicated in green.

From Figure 17, it can be seen that two adjacent batteries, Cell6 and Cell7, can form a high-energy cell cluster. Figure 18a shows the simulation results of the AC2AC balancing strategy, which shows that the highest SOC battery is balancing with the lowest SOC battery. The equalization time is 662s, and the SOC of each battery after equalization is 43.49, 43.79, 43.49, 44.49, 44.49, 44.49, 44.49 and 43.49, with an average of 44.0275 and the variance of 0.2223. Figure 18b shows the simulation results of the MC2AC equalization strategy. It can be seen that, at time $0 \sim t1$, the high-energy battery cluster formed by Cell6 and Cell7 balances the lowest SOC battery. After time $t1$, since Cell6 has finished equalizing, Cell6 and Cell7 can no longer form the high-energy battery cluster, and the subsequent equalization is transferred to the AC2AC equalization process, where $t1$ is 180.228 s. The equalization time is 557.126 s, and the SOC of each battery after equalization is 43.54, 43.8, 43.54, 44.54, 44.49, 44.54, 44.54 and 43.54, with an average of 44.06625 and the variance of 0.2193. The comparison of the two control strategies is shown in Table 3.

As can be seen from the above, compared with the AC2AC equalization strategy, MC2AC equalization has the following advantages. (1) It can effectively shorten the equalization time and increase the time efficiency by 15.842%. (2) The variance is reduced by 1.35%, indicating that the equalization results are less discrete and the results are more stable. (3) Due to the shortened equalization time, the energy efficiency is not reduced but slightly increased by 0.088%.

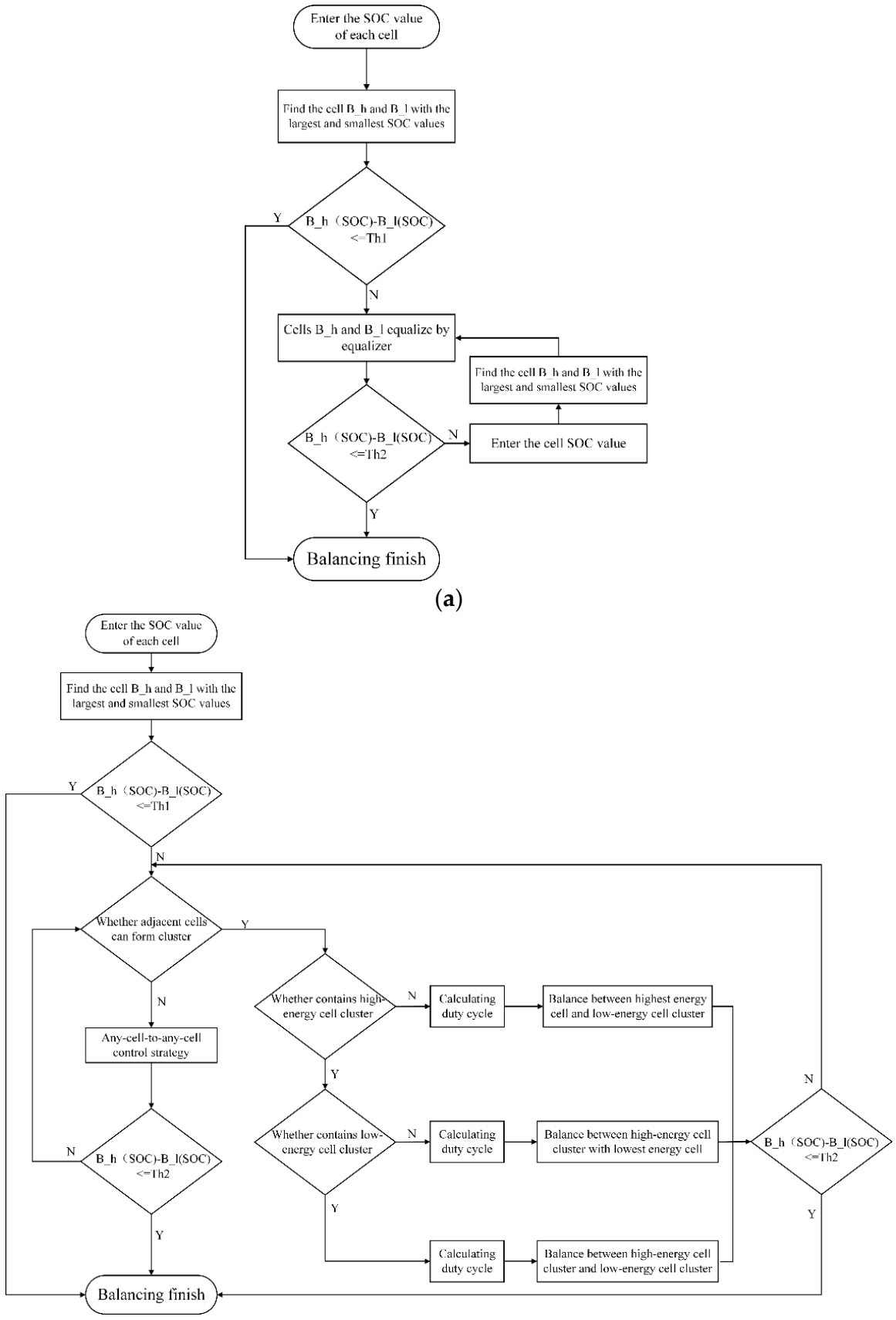

Figure 16. (**a**). Any-cell-to-any-cell control strategy. (**b**). Multi-cell-to-multi-cell control strategy.

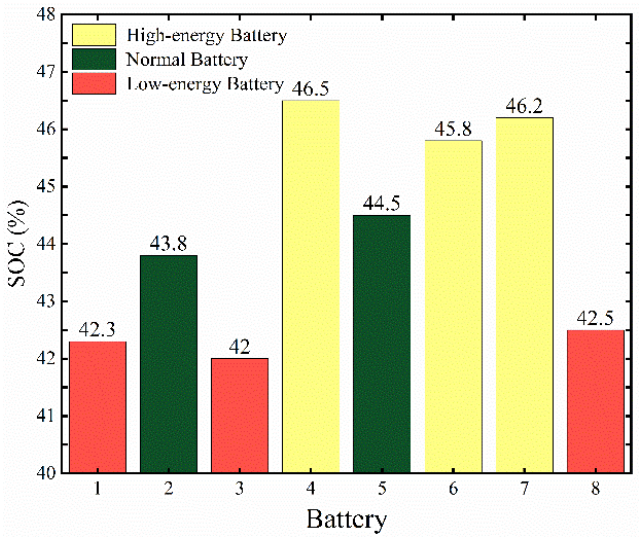

Figure 17. Battery pack energy state distribution.

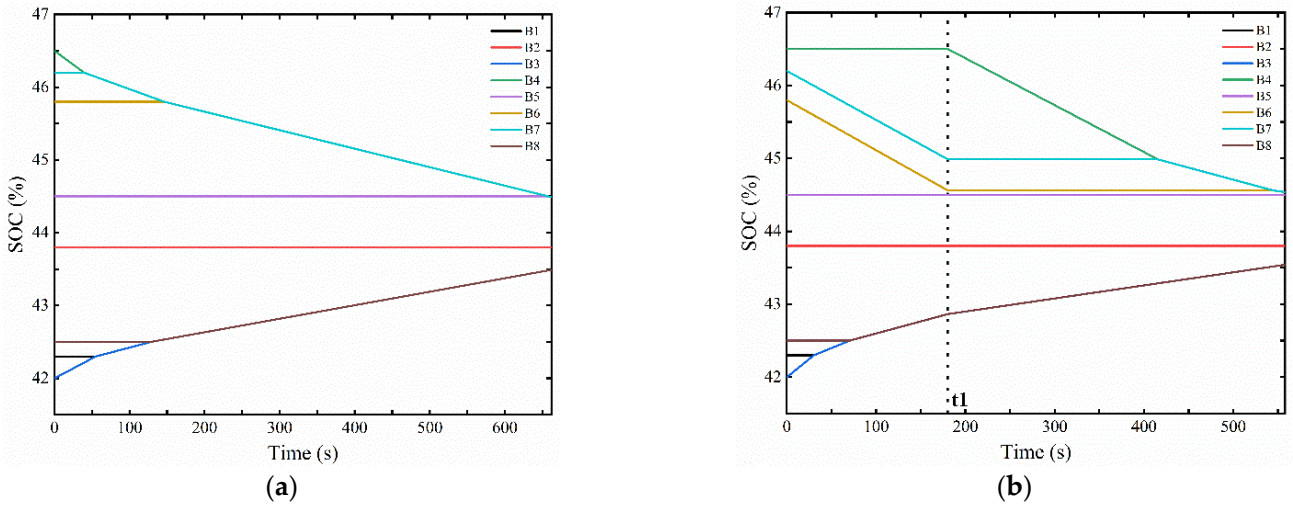

Figure 18. (**a**) AC2AC equalization simulation results (**b**) MC2AC equalization simulation results.

Table 3. Equalization results for AC2AC and MC2AC control strategies.

Equalization Strategy	After Equalization					
	The SOC of Each Cell		Average	Range	Variance	Time (s)
AC2AC Equalization	43.49 43.79 43.49 44.49	44.49 44.49 44.49 43.49	44.0275	1	0.2223	662
MC2AC Equalization	43.54 43.8 43.54 44.54	44.49 44.54 44.54 43.54	44.06625	1	0.2193	557.126

4.3. Multi-Cell-to-Multi-Cell Simulation Verification

Assuming that the SOC values of the eight series batteries are 43.8, 42.3, 42.5, 46.5, 44.5, 45.8, 46.2 and 42, respectively, the energy state distribution diagram of the battery pack is shown in Figure 19. Among them, yellow represents the high-energy battery, green represents the normal battery, and red represents the low-energy battery.

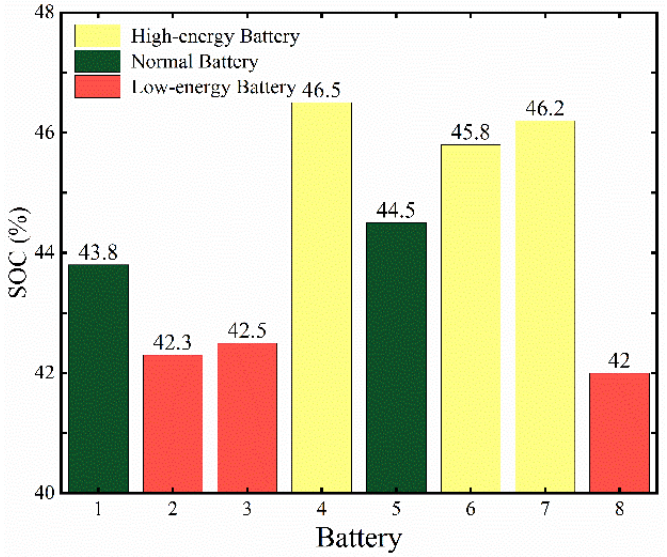

Figure 19. Battery pack energy state distribution.

From Figure 19, it can be seen that two adjacent batteries, Cell6 and Cell7, can form a high-energy cell cluster, and Cell2 and Cell3 can form a low-energy cell cluster. Figure 20a shows the simulation results of the AC2AC balancing strategy, which shows that the highest SOC battery is balancing with the lowest SOC battery. The equalization time is 662 s, and the SOC of each battery after equalization is 43.8, 43.49, 43.49, 44.49, 44.49, 44.49, 44.49 and 43.49, with an average of 44.02875 and the variance of 0.2218. Figure 20b shows the simulation results of the MC2MC equalization strategy. It can be seen that, at time $0 \sim t1$, the high-energy battery cluster formed by Cell6 and Cell7 balances the low-energy battery cluster formed by Cell2 and Cell3. At time $t1 \sim t2$, since Cell6 has finished equalizing, Cell6 and Cell7 can no longer form the high-energy battery cluster. The subsequent equalization is transferred to the AC2MC balancing process; the highest SOC battery balances the low-energy battery cluster formed by Cell2 and Cell3. After time $t2$, since Cell3 has finished equalizing, Cell2 and Cell3 can no longer form the low-energy battery cluster, and the subsequent equalization is transferred to the AC2AC equalization process, where the equalization turning points $t1$ and $t2$ are 88.037 s and 157.458 s respectively. The equalization time is 467.379 s, and the SOC of each battery after equalization is 43.8, 43.54, 43.63, 44.54, 44.49, 44.54, 44.54 and 43.54, with an average of 44.0775, and the variance of 0.2084. The comparison of the two equalization strategies is shown in Table 4.

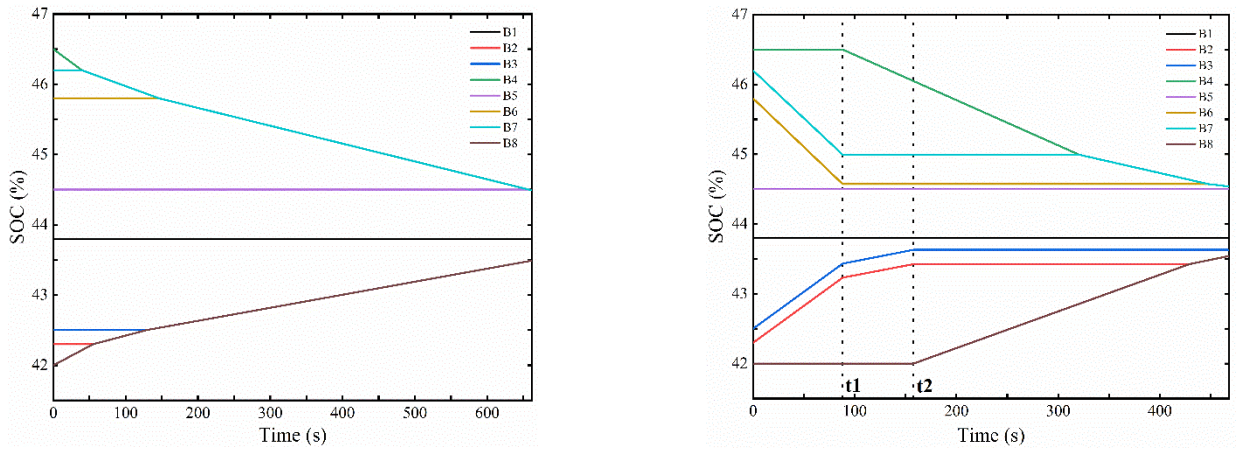

Figure 20. (**a**) AC2AC equalization simulation results (**b**) MC2MC equalization simulation results.

Table 4. Equalization results for AC2AC and MC2MC control strategies.

Equalization Strategy	After Equalization					
	The SOC of Each Cell		Average	Range	Variance	Time (s)
AC2AC Equalization	43.8	44.49	44.02875	1	0.2218	662
	43.49	44.49				
	43.49	44.49				
	44.49	43.49				
MC2MC Equalization	43.8	44.49	44.0775	1	0.2084	467.379
	43.54	44.54				
	43.63	44.54				
	44.54	43.54				

As can be seen from the above, compared with the AC2AC equalization strategy, MC2MC equalization has the following advantages. (1) It can effectively shorten the equalization time and increase the time efficiency by 29.4%. (2) The variance is reduced by 6.04%, indicating that the equalization results are less discrete and the results are more stable. (3) Due to the shortened equalization time, the energy efficiency is not reduced but slightly increased by 0.1107%.

5. Conclusions

This paper proposes an active balancing scheme for battery packs to achieve multi-cell-to-multi-cell balancing. The operation principle of the balancing topology combining the Buck-Boost circuit and switch array is analyzed in detail, and the accuracy of the simulation model is verified. In addition, to explore the influence of various factors on the equalization effect, the switching frequency and voltage difference are selected for analysis and calculation. The results show that the larger the switching frequency is, the smaller the average equalization current and heat loss rate are. Therefore, considering the time efficiency and energy efficiency, the switching frequency should be about 10 KHz. Voltage difference significantly affects the duty cycle, so it is absolutely necessary to introduce a variable duty cycle in MC2MC equalization. Using three batteries and two batteries to balance one battery results in a 58.35% and 46.2% improvement in time efficiency over using only one battery to balance one battery, respectively. Finally, eight batteries are selected to build the simulation model. Under the condition that each battery's initial state of charge is the same, but the location is different, compared with any-cell-to-any-cell (AC2AC) equalization, the time efficiency of multi-cell-to-multi-cell equalization is increased by 15.842% and 29.4%, respectively. The variance is reduced by 1.35% and 6.04%, respectively, and because the equalization time is shortened, the energy efficiency is slightly improved.

Author Contributions: Conceptualization, S.L.; software, S.L.; validation, H.W. and S.L.; formal analysis, H.W.; writing—original draft preparation, S.L.; writing—review and editing, H.W. and D.Q.; visualization, T.W. and J.C.; supervision, H.W.; project administration, T.W.; funding acquisition, D.Q. All authors have read and agreed to the published version of the manuscript.

Funding: This research was funded by the National Key R&D Program—Research on key technologies of N2/N3 pure electric commercial vehicle power platform and vehicle application (2018YFB0106204).

Data Availability Statement: Data is contained within the article.

Conflicts of Interest: The authors declare no conflict of interest.

References

1. Zhang, Y. Clean Energy: Opportunities and Challenges. *Engineering* **2017**, *3*, 431. [CrossRef]
2. Gu, D. Dedication to Clean Power and Promotion of the Energy Revolution. *Engineering* **2020**, *6*, 1331–1332. [CrossRef]
3. Davis, L. Clean Energy Perspective. *Engineering* **2017**, *3*, 782. [CrossRef]

4. Li, S.; He, J.; Guo, Z. A Novel Lithium-ion Battery Active Equalization Structure and its Control Strategy Based on Bidirectional Converter Unit. In Proceedings of the 2018 IEEE International Power Electronics and Application Conference and Exposition (PEAC), Shenzhen, China, 4–7 November 2018; pp. 1–5.
5. Zhang, E.; Xu, C.; Liu, G.; Jiang, K.; Wang, K. An active battery equalization scheme for Lithium iron phosphate batteries. *Energy Procedia* **2019**, *158*, 4702–4707. [CrossRef]
6. Dam, S.; John, V. A Multi-Active-Half-Bridge Converter based Soft-switched Fast Voltage Equalizer for Multi-cell to Multi-cell Charge Transfer. In Proceedings of the 2019 IEEE Transportation Electrification Conference (ITEC-India), Bengaluru, India, 17–19 December 2019; pp. 1–6.
7. A Hannan, M.; Hoque, M.; Peng, S.E.; Uddin, M.N. Lithium-ion battery charge equalization algorithm for electric vehicle applications. *IEEE Trans. Ind. Appl.* **2017**, *53*, 2541–2549. [CrossRef]
8. Zhang, C.; Shang, Y.; Li, Z.; Cui, N. An Interleaved Equalization Architecture with Self-Learning Fuzzy Logic Control for Series-Connected Battery Strings. *IEEE Trans. Veh. Technol.* **2017**, *66*, 10923–10934. [CrossRef]
9. Ji, L.; Yang, C.; Fathy, H. Nonlinear Model-Predictive Optimal Control of an Active Cell-to-Cell Lithium-Ion Battery Pack Balancing Circuit. *IFAC* **2017**, *50*, 14483–14488.
10. Feng, F.; Hu, X.; Liu, J.; Lin, X.; Liu, B. A review of equalization strategies for series battery packs: Variables, objectives, and algorithms. *Renew. Sust. Energ. Rev.* **2019**, *116*, 109464. [CrossRef]
11. Zhang, S.; Yang, L.; Zhao, X.; Qiang, J. A GA optimization for lithium-ion battery equalization based on SOC estimation by NN and FLC. *Int. J. Electr. Power Energy Syst.* **2015**, *73*, 318–328. [CrossRef]
12. Tudoroiu, R.-E.; Zaheeruddin, M.; Tudoroiu, N.; Radu, S.-M. SOC Estimation of a Rechargeable Li-Ion Battery Used in Fuel-Cell Hybrid Electric Vehicles—Comparative Study of Accuracy and Robustness Performance Based on Statistical Criteria. Part I: Equivalent Models. *Batteries* **2020**, *6*, 42. [CrossRef]
13. Tudoroiu, R.-E.; Zaheeruddin, M.; Tudoroiu, N.; Radu, S.-M. SOC Estimation of a Rechargeable Li-Ion Battery Used in Fuel Cell Hybrid Electric Vehicles—Comparative Study of Accuracy and Robustness Performance Based on Statistical Criteria. Part II: SOC Estimators. *Batteries* **2020**, *6*, 41. [CrossRef]
14. Song, L.; Liang, T.; Lu, L.; Ouyang, M. Lithium-ion battery pack equalization based on charging voltage curves. *Int. J. Electr. Power Energy Syst.* **2020**, *115*, 105516. [CrossRef]
15. Li, K.; Zong, X.; Liu, Q.; Sun, Y.; Xue, F. Design of an Active Battery Equalization Circuit with DC-DC Converter. In Proceedings of the 2021 3rd Asia Energy and Electrical Engineering Symposium (AEEES), Chengdu, China, 26–29 March 2021; pp. 863–866.
16. Zhang, H.; Wang, Y.; Qi, H.; Zhang, J. Active Battery Equalization Method Based on Redundant Battery for Electric Vehicles. *IEEE Trans. Veh. Technol.* **2019**, *68*, 7531–7543. [CrossRef]
17. Park, S.; Park, K.; Kim, H.; Moon, G.; Youn, M. Single-Magnetic Cell-to-Cell Charge Equalization Converter with Reduced Number of Transformer Windings. *IEEE Trans. Power Electron.* **2011**, *27*, 2900–2911. [CrossRef]
18. Ma, Y.; Duan, P.; Sun, Y.; Chen, H. Equalization of Lithium-Ion Battery Pack Based on Fuzzy Logic Control in Electric Vehicle. *IEEE Trans. Ind. Electron.* **2018**, *65*, 6762–6771. [CrossRef]
19. Li, Y.; Xu, J.; Mei, X.; Wang, J. A Unitized Multiwinding Transformer-Based Equalization Method for Series-Connected Battery Strings. *IEEE Trans. Power Electron.* **2019**, *34*, 11981–11989. [CrossRef]
20. Pascual, C.; Krein, P.T. Switched capacitor system for automatic series battery equalization. In Proceedings of the APEC 97—Applied Power Electronics Conference, Atlanta, GA, USA, 27 February 1997; Volume 2, pp. 848–854.
21. Lee, Y.; Cheng, M. Intelligent control battery equalization for series connected lithium-ion battery strings. *IEEE Trans. Ind. Electron.* **2005**, *52*, 1297–1307. [CrossRef]
22. Daowd, M.; Antoine, M.; Omar, N.; Van den Bossche, P.; Van Mierlo, J. Single Switched Capacitor Battery Balancing System Enhancements. *Energies* **2013**, *6*, 2149–2174. [CrossRef]
23. Li, S.; Mi, C.; Zhang, M. A High-Efficiency Active Battery-Balancing Circuit Using Multiwinding Transformer. *IEEE Trans. Ind. Appl.* **2012**, *49*, 198–207. [CrossRef]
24. Kutkut, N.; Wiegman, H.; Divan, D.; Novotny, D. Design considerations for charge equalization of an electric vehicle battery system. *IEEE Trans. Ind. Appl.* **1999**, *35*, 28–35. [CrossRef]
25. Liu, Y.; Xia, C.; Gu, M.; Xin, W.; Men, X. A novel active equalizer for Li-ion battery pack in electric vehicles. *Energy Procedia* **2019**, *158*, 2649–2654. [CrossRef]
26. Shang, Y.; Xia, B.; Zhang, C.; Cui, N.; Yang, J.; Mi, C. An Automatic Equalizer Based on Forward-Flyback Converter for Series-Connected Battery Strings. *IEEE Trans. Ind. Electron.* **2017**, *64*, 5380–5391. [CrossRef]
27. Shang, Y.; Cui, N.; Zhang, C. An Optimized Any-Cell-to-Any-Cell Equalizer Based on Coupled Half-Bridge Converters for Series-Connected Battery Strings. *IEEE Trans. Power Electron.* **2018**, *34*, 8831–8841. [CrossRef]
28. Daowd, M.; Omar, N.; Van den Bossche, P.; Van Mierlo, J. A Review of Passive and Active Battery Balancing Based on MATLAB/Simulink. *Int. Rev. Electr. Eng.-IREE.* **2011**, *6*, 2974–2989.
29. Das, U. Advancement of lithium-ion battery cells voltage equalization techniques: A review. *Renew. Sust. Energ. Rev.* **2020**, *134*, 110227. [CrossRef]
30. Wang, B.; Qin, F.; Zhao, X.; Ni, X.; Xuan, D. Equalization of series connected lithium-ion batteries based on back propagation neural network and fuzzy logic control. *Int. J. Energy Res.* **2020**, *44*, 4812–4826. [CrossRef]

31. Wu, X.; Cui, Z.; Li, X.; Du, J.; Liu, Y. Control Strategy for Active Hierarchical Equalization Circuits of Series Battery Packs. *Energies* **2019**, *12*, 2071. [CrossRef]
32. Wang, S.; Yang, S.; Yang, W.; Wang, Y. A New Kind of Balancing Circuit With Multiple Equalization Modes for Serially Connected Battery Pack. *IEEE Trans. Ind. Electron.* **2020**, *68*, 2142–2150. [CrossRef]
33. Chen, Y. An any-cell(s)-to-cell(s) equalization method with a single magnetic component for Lithium-ion battery pack. *J. Energy Storage* **2020**, *33*, 102071. [CrossRef]
34. Wu, T.; Qi, Y.; Liao, L.; Ji, F.; Chen, H. Research on equalization strategy of lithium-ion batteries based on fuzzy logic control. *J. Energy Storage* **2021**, *40*, 102722. [CrossRef]
35. Shang, Y.; Zhang, Q.; Cul, N.; Duan, B.; Zhou, Z.; Zhang, C. Multicell-to-Multicell Equalizers Based on Matrix and Half-Bridge *LC* Converters for Series-Connected Battery Strings. *IEEE J. Emerg. Sel. Top. Power Electron.* **2019**, *8*, 1755–1766. [CrossRef]